Photoacoustics 31 (2023) 100518

Contents lists available at ScienceDirect

Photoacoustics

journal homepage: www.elsevier.com/locate/pacs

Assessment of vibrational-translational relaxation dynamics of in a wet-nitrogen matrix through QEPAS

Mariagrazia Olivieri [a,b,1], Marilena Giglio [a,1], Stefano Dello Russo [c], Giansergio Menduni [b], Andrea Zifarelli [b], Pietro Patimisco [b], Angelo Sampaolo [b], Hongpeng Wu [a], Lei Dong [a,*], Vincenzo Spagnolo [a,b,*]

[a] State Key Laboratory of Quantum Optics and Quantum Optics Devices, Institute of Laser Spectroscopy, Shanxi University, Taiyuan 030006, China
[b] PolySense Lab - Dipartimento Interateneo di Fisica, Politecnico and University of Bari, Via Amendola 173, Bari, Italy
[c] Italian Space Agency (ASI), Centro di geodesia Spaziale "Giuseppe Colombo", Matera, Italy

ARTICLE INFO

Keywords:
Methane isotopologues
Relaxation rates
Quartz-enhanced photoacoustic spectroscopy
Trace gas sensing
Quantum cascade laser

ABSTRACT

Here we report on a study of the non-radiative relaxation dynamic of $^{12}CH_4$ and $^{13}CH_4$ in wet nitrogen-based matrixes by using the quartz-enhanced photoacoustic spectroscopy (QEPAS) technique. The dependence of the QEPAS signal on pressure at fixed matrix composition and on H_2O concentration at fixed pressure was investigated. We demonstrated that QEPAS measurements can be used to retrieve both the effective relaxation rate in the matrix, and the V-T relaxation rate associated to collisions with nitrogen and water vapor. No significant differences in measured relaxation rates were observed between the two isotopologues.

1. Introduction

The concentration of methane (CH_4) in atmosphere is currently around two-and-a-half times greater than pre-industrial levels and is increasing steadily. This rise has important implications for climate change, since methane is the second most abundant greenhouse gas following carbon dioxide and accounting for 30 % of the increase in the global temperature. It was estimated that at a 20-year timescale total global emissions of methane are equivalent to over 80 % of global carbon dioxide emissions [1]. Moreover, CH_4 is a potent local air pollutant and the primary contributor to the formation of ground-level ozone [2]. CH_4 emissions can be grouped into three categories: biogenic, pyrogenic, and thermogenic. Biogenic CH_4 is mainly produced by microbes found in wetlands, rice paddies, oxygen-poor freshwater reservoirs, digestive systems of ruminants and termites, sewages, landfills. Pyrogenic CH_4 is a result of the incomplete combustion of biomass, biofuels, and fossil fuels. Thermogenic CH_4 has been produced over time by geological processes and has been introduced into the environment via natural processes such as mud volcanoes, terrestrial and marine seeps, or human activities, as fossil fuels extractions, coal mining activities, bioenergy production [3,4]. Thus, within these categories, a distinction can be made between natural and anthropogenic sources. The 2022 update of the IEA Global Methane Tracker estimated that the huger contribute for anthropogenic CH_4 emissions comes from the agriculture activities and the energy sector [5].

Based on their emission source, methane samples have different isotopic signatures in terms of $\delta^{13}C$, that is the deviation of the isotopic ratio $^{13}CH_4/^{12}CH_4$ (R) with respect to a standard ratio (R_{st}) expressed in part per thousand, i.e., $\delta^{13}C[‰]=(R-R_{st})/R_{st}*1000$. Typically, $\delta^{13}C$ ranges from − 55 to − 70‰ for biogenic emissions, − 25 to − 55‰ for thermogenic emissions, and − 13 to − 25‰ for pyrogenic emissions [4]. As a result, the isotopic abundance of a CH_4 sample represents a fingerprint of its emission source. Moreover, $\delta^{13}C$ measurement can be employed as a guide for downstream operations in petrochemical industry. This parameter, together with the ratio of methane to higher hydrocarbons concentration (ethane and propane), allows the reconstruction of the Bernard graph, employed to determine the origin of natural gas seeps overlying possible oil reservoirs: petrogenic processes lead to mixtures containing higher molecular weight hydrocarbons and $\delta^{13}C$ with negative value higher than –50‰ [6,7]. Isotopic ratio measurements can also be used to study the dynamics of natural gas reservoirs by quantifying the carbon isotope fractionation resulting from

* Corresponding authors at: State Key Laboratory of Quantum Optics and Quantum Optics Devices, Institute of Laser Spectroscopy, Shanxi University, Taiyuan 030006, China.
E-mail addresses: donglei@sxu.edu.cn (L. Dong), v.spagnolo@poliba.it (V. Spagnolo).
[1] These authors contributed equally to this work.

https://doi.org/10.1016/j.pacs.2023.100518
Received 23 March 2023; Received in revised form 4 May 2023; Accepted 31 May 2023
Available online 2 June 2023

molecular diffusion of methane in water-saturated sedimentary rocks [8]. However, directional drilling and hydraulic fracturing can negatively impact on groundwater quality, causing CH_4 contamination of aquifers overlying shale formations. Therefore $\delta^{13}C$ measurements can be employed to identify the contamination source: drinking-water contaminated samples characterized by less negative $\delta^{13}C$ values are associated with nearby active sites [9,10]. Moreover, evidences of methane production under aerobic conditions in eukaryotes, such as plants, animals, algae or fungi and studies about their isotopic signature are reported in literature [11,12]. Finally, CH_4 detection and isotopic ratio measurements also play an important role in research about planet's atmosphere, providing indications on the nature of emission source [13,14].

Isotopic composition is typically measured by collecting samples that are subsequently analyzed with Gas chromatography–mass spectrometry (GC-MS) systems [15,16]. However, the use of sensors in harsh environment and the ease of deployment in different scenarios of in situ measurements require a high level of robustness and compactness, hardly achievable with GC-MS systems. Laser-based spectroscopic techniques already demonstrated highly sensitive and selective detection of several gas species [17–20], including hydrocarbons and their isotopologues [21–23]. Quartz-enhanced photoacoustic spectroscopy (QEPAS) helped in developing small sized sensors with the additional advantage of offering a high level of modularity. QEPAS is an evolution of photoacoustic spectroscopy (PAS) and employs a quartz tuning fork (QTF) as a sharply resonant acoustic transducer to detect acoustic waves generated by the target gas molecules absorbing modulated laser light and relaxing energy via non-radiative processes, i.e., via collisions with the surrounding molecules [24–26]. QEPAS and PAS were demonstrated as leading techniques for CH_4 detection in wet and dry nitrogen-based matrixes [27–30], in samples containing both nitrogen and oxygen [31] or in air [32,33]. The possibility of performing multi-gas detection employing a single sensor was also exploited: methane was detected together with several infrared absorbers such as ammonia, oxides of nitrogen, water vapor, hydrogen sulfide for several applications like breath analysis, environmental monitoring, gas leaks detection in natural gas plants [34–37], production monitoring during petroleum exploration, both at trace level and high concentration [38–44].

A common thread of PAS-based spectroscopy techniques is the dependence of the sensor responsivity on the gas matrix composition, whose variations can affect the dynamics of a target molecule energy relaxation through its collisional partners, affecting in turn the photoacoustic generation [31,45–47]. Therefore, the assessment of the QEPAS signal dependence on the excited molecule relaxation rates is a crucial requirement for QEPAS detection of $^{13}CH_4$ and $^{12}CH_4$ abundances and to enable high precision $\delta^{13}C$ measurements, which range between − 60‰ and − 50‰ for natural gas samples. Variation in the calculated isotopic ratio caused by matrix fluctuations rather than by drifts in the isotopologue concentration must be recognized and filtered out to increase both the precision and the accuracy of the measurement. Several approaches have been proposed to compute and compensate for the effect of non-radiative relaxation processes on PA signal, mainly relying on i) continuous monitoring of different analyte concentrations and physical parameters during the measurements, with a subsequent implementation of complex algorithms [33,48], and/or ii) multivariate analysis of extended photoacoustic spectra [49]. A knowledge of methane isotopologues relaxation dynamics could be extremely useful to predict the influence of matrix fluctuations on the isotopic ratio measurement. Dello Russo et al. demonstrated the possibility of employing a standard QEPAS setup to estimate the effective relaxation rate of methane [50]. The measured value was in excellent agreement with those reported in literature, generically associated to a standard sample of CH_4, i.e., containing natural abundances of each isotopologue. However, $^{12}CH_4$ and $^{13}CH_4$ have a mass difference due to the additional neutron in the second one, resulting in a ~10 cm^{-1} shift between the isotopologues energy levels [51].

In the presented work, the method proposed by Dello Russo et al. is more extensively applied to retrieve the vibrational-translational relaxation rates associated to the collisions of each methane isotopologue in the simplest methane gas mixture that can be analyzed in nature, i.e., $^{13}CH_4$ and $^{12}CH_4$ with the main collisional partners in the infrared range: water vapor (H_2O) and nitrogen (N_2). In detail, the relaxation rates of $^{13}CH_4$ and $^{12}CH_4$ colliding with H_2O and N_2 are measured, to determine whether the isotopologues mass difference and the consequent energy levels shift may cause a difference in their relaxation velocities.

2. Influence of V-T relaxation processes on QEPAS signal

When infrared incident photons are absorbed by molecules, rotational-vibrational levels are excited. De-excitation will occur mainly through non radiative processes, since energy is too small for chemical processes, and radiative lifetimes are long (10^{-1}-10^{-3} s) compared to non-radiative processes (10^{-6}-10^{-9} s) in the pressure range used in PAS spectroscopy (10–760 Torr) [52]. Thus, the absorbed energy can be directly converted into kinetic energy through collision-induced vibrational-to-translation relaxation (V-T) or transferred as vibrational energy to molecules having vibrational states of similar energy, through collision-induced vibrational-to-vibrational relaxation (V-V). Therefore, heat is released within the gas sample as a result of the energy transfer from internal to translational molecular degrees of freedom, which depends on the number of collisions experienced by one molecule per second, namely the relaxation rate k. Modulation of the laser light at frequency f causes a sequence of local heating and cooling within gas, generating sound waves. In QEPAS, the QTF detects the photoacoustic waves and converts them into an electrical signal. The QTF quality factor has a strong dependence on pressure p [53].

Thus, the QEPAS signal S depends on i) the laser optical power P_L exciting the target gas molecules, ii) the radiation-to-sound conversion efficiency $\varepsilon(f,k,p)$, iii) the QTF quality factor $Q(p)$, iv) the absorption cross-section $\sigma(p)$:

$$S(f,k,p) = \zeta P_L \varepsilon(k,f,p) Q(p) \sigma(p), \tag{1}$$

where ζ is a sensor constant. The dependence of $\sigma(p)$ on pressure can be neglected as it provides a nearly constant value [54].

The radiation-to-sound conversion efficiency $\varepsilon(f,k,p)$ can be evaluated by computing the total heat production rate from all the excited states involved in the relaxation process [48]. In the simplest hypothesis that only V-T relaxation of the excited state to the ground state occurs, $\varepsilon(f,k,p)$ can be expressed as [30,55]:

$$\varepsilon(f,k,p) = \frac{1}{\sqrt{1+\left(\frac{2\pi f}{kp}\right)^2}}. \tag{2}$$

Therein k is the effective relaxation rate, measured in $Torr^{-1}s^{-1}$ and defined as the sum of the V-T relaxation rates associated to each collision in the mixture, weighted by the related concentration [31,50].

Let's now consider a gas mixture composed of CH_4, H_2O and N_2. When methane is optically excited in the mid-infrared at 1296 cm^{-1}, the ν_4 mode in the first polyad (dyad) is excited. V-T relaxation of excited CH_4* molecules can be analyzed through a simplified model assuming the de-excitation occurring via one-stage collisions with H_2O, N_2 and CH_4 [29,30] molecules. The relaxation rates associated to V-T paths are reported in Table 1.

The methane effective relaxation rate can be written as:

$$k = k_{N_2} C_{N_2} + k_{H_2O} C_{H_2O} + k_{CH_4} C_{CH_4}, \tag{3}$$

where each C_P and k_P represents the absolute concentration of the collisional partner P (N_2, H_2O or CH_4) and the path-related energy relaxation rate. Based on the relaxation rate values reported in Table 1, for wet (0.1–1 % absolute humidity) mixtures containing low methane

Table 1
V-T relaxation rates (k_P) associated to the collisions between CH_4 molecules in the ν_4 excited state and the collisional partner P, i.e., H_2O, N_2 or CH_4.

Collisional partner P	Relaxation path	k_P ($s^{-1}Torr^{-1}$)	Ref.
H_2O	$CH_4^*(\nu_4) + H_2O \xrightarrow{k_{H_2O}} CH_4 + H_2O$	1.32 * 10^5	[30]
N_2	$CH_4^*(\nu_4) + N_2 \xrightarrow{k_{N_2}} CH_4 + N_2$	1.05 * •10^2	[56]
CH_4	$CH_4^*(\nu_4) + CH_4 \xrightarrow{k_{CH_4}} CH_4 + CH_4$	1.05 * •10^3	[56]

concentration, i.e., in the 0.1 % range, the terms $k_{N_2}C_{N_2}$, $k_{H_2O}C_{H_2O}$ and $k_{CH_4}C_{CH_4}$ are in the order of 10^2 $s^{-1}Torr^{-1}$, 10^3-10^2 $s^{-1}Torr^{-1}$ and 10^0 $s^{-1}Torr^{-1}$ respectively. This demonstrates that the term due to self-collisions can be neglected for methane at trace-level in wet nitrogen. Methane in natural abundance is composed of 98.9 % of $^{12}CH_4$ and 1.1 % of $^{13}CH_4$. Therefore, when methane ν_4 mode is excited, energy relaxation paths for each isotopologue must be considered. Excited $^{12}CH_4$* V-T relaxation occurs via collisional paths with H_2O, $^{13}CH_4$, N_2 and $^{12}CH_4$ itself [30]. A similar relaxation scheme can be considered for excited $^{13}CH_4$* . Based on Eq. (3), the effective relaxation rate for the methane isotopologue I ($^{12}CH_4$ or $^{13}CH_4$) can be written as:

$$k^I = k^I_{N_2}C_{N_2} + k^I_{H_2O}C_{H_2O} + k^I_{^{12}CH_4}C_{^{12}CH_4} + k^I_{^{13}CH_4}C_{^{13}CH_4} \tag{4}$$

As discussed, assuming $k^I_{^{12}CH_4}C_{^{12}CH_4} \approx k^I_{^{13}CH_4}C_{^{13}CH_4} \approx 0$, Eq. (4) can be approximated as:

$$k^I \approx k^I_{N_2}C_{N_2} + k^I_{H_2O}C_{H_2O} \tag{5}$$

From Eqs. (1) and (2), the effective relaxation rate trend can be retrieved by measuring the ratio between the QEPAS signal and the QTF quality factor, as a function of pressure [50]. Let's introduce the frequency-related parameter A^I expressed in terms of effective relaxation rate:

$$A^I = \frac{2\pi f}{k^I} \tag{6a}$$

or in terms of V-T relaxation rates:

$$A^I \approx \frac{2\pi f}{k^I_{N_2}C_{N_2} + k^I_{H_2O}C_{H_2O}} \tag{6b}$$

Therefore, the ratio S/Q as a function of pressure can be written as:

$$\frac{S(p)}{Q(p)} \approx \frac{z_1}{\sqrt{1 + \left(\frac{A^I}{p}\right)^2}}, \tag{7}$$

where z_1 contains all the pressure-independent contributes to the QEPAS signal.

Also, Eqs. (1–4) can be rearranged to analyze the dependence of the radiation to sound conversion efficiency on the concentration of the gas mixture components, at a fixed pressure. In a mixture of a low concentration of the isotopologue I in a wet nitrogen matrix and with a negligible variation of the QTF quality factor with the water concentration, the I-QEPAS signal as a function of the H_2O concentration C_{H_2O} for a pressure $p = p_0$ is given by:

$$S(C_{H_2O}) \approx \frac{z_2}{\sqrt{1 + \left(\frac{k^I_{N_2} p_0}{2\pi f} (1 - C_{H_2O} - C_I) + \frac{k^I_{H_2O} p_0}{2\pi f} C_{H_2O} \right)^{-2}}} = \frac{z_2}{\sqrt{1 + \left(B^I_{N_2}(1 - C_{H_2O} - C_I) + B^I_{H_2O}C_{H_2O} \right)^{-2}}}, \tag{8}$$

where $B^I_{N_2} = k^I_{N_2}p_0/2\pi f$, $B^I_{H_2O} = k^I_{H_2O}p_0/2\pi f$ and z_2 contains all the water-independent contributes (and therefore also $Q(p_0)$) and represents the saturated QEPAS signal at high water concentration. Eq. (8) shows that the analysis of the QEPAS signal as a function of the H_2O concentration can be also exploited to retrieve $k^I_{H_2O}$ and $k^I_{N_2}$.

3. Experimental setup

The experimental setup used to measure the relaxation rates of methane isotopologues in a wet nitrogen-based matrix is depicted in Fig. 1.

The QTF was hold inside the Acoustic Detection Module (ADM), i.e., a vacuum-tight stainless-steel cell with fittings for gas inlet and outlet equipped with two ZnSe 7–12 μm antireflection (AR) coated windows to transmit the laser light. Methane molecules were excited using a distributed-feedback quantum cascade laser (DFB-QCL) with center emission at ~ 7.719 μm. The laser temperature was controlled by a thermoelectric cooler (TEC), whereas a current driver (CD) provided current to the QCL. The laser beam was focused between the QTF prongs inside the ADM by using a plano-convex ZnSe lens with a focal length of 75 mm and a 7–12 μm AR coating. The ADM was placed on a 5-axis stage for alignment purposes. The laser power passing through the ADM was measured by a power meter (PM) set behind the ADM also for alignment purposes. The QTF piezoelectric current signal was converted into a voltage signal by a transimpedance amplifier (feedback resistor 10 MΩ). A multifunction I/O device (model NI USB 6361) and a LabVIEW-based software were employed to electrically characterize the QTF and to perform QEPAS measurements.

For QTF electrical characterization, the analog output AO1 provided a sinusoidal voltage excitation for the QTF, while for QEPAS measurements the analog output AO0 provided a dither to the laser current driver at half of the QTF resonance frequency f, to perform wavelength modulation, added to a slow ramp, to scan the laser current across the gas target absorption peak. In both cases, the generated signals were also used as a reference for the lock-in demodulation. The QTF transduced signal was acquired through the analog input AI2. For QTF electrical characterization the signal was demodulated at the excitation frequency using the reference signal acquired thorough the analog input AI1, while for QEPAS measurements the signal was demodulated at the resonance frequency f using the reference signal acquired thorough the analog input AI0. The 2f-signal resembles the second derivative of the absorption cross-section line-shape distorted by a residual amplitude modulation, proportional to the first derivative but not affecting the peak intensity [57].

Measurements were performed using two gas cylinders, one containing a certified concentration of 1000 ppm of $^{13}CH_4$ in N_2 and the other containing a certified concentation of 1000 ppm of $^{12}CH_4$ in N_2. The mixture was humidified using a 1000 cm^2 silicone membrane hollow fiber gas exchanger (PermSelect). When the gas stream enters the port on one end cap of the membrane gas humidifier and flows through the silicone hollow fiber, water fills the shell side of the humidifier (outside of the hollow fiber), and permeate through silicone, thereby humidifying the gas stream.

The gas flow was controlled via a valve-system. The pressure in the gas line was set using a vacuum pump and a pressure controller. Gas temperature and relative humidity inside the line were monitored using a Testo 635–2 thermohygrometer equipped with a humidity probe and connected to the personal computer for data acquisition.

A set of five custom QTFs was chosen to measure the effective relaxation rate of methane isotopologues using the method proposed in [50]. QTF with I- or T-shaped prongs, with or without grooves carved on the surfaces were properly selected to analyze the QEPAS signal obtained by exciting methane molecules with modulation frequencies ranging between 3 kHz and 15 kHz, with a step of about 3 kHz, A schematic of the employed QTFs is shown in Fig. 2(a). QTF I0.8 was

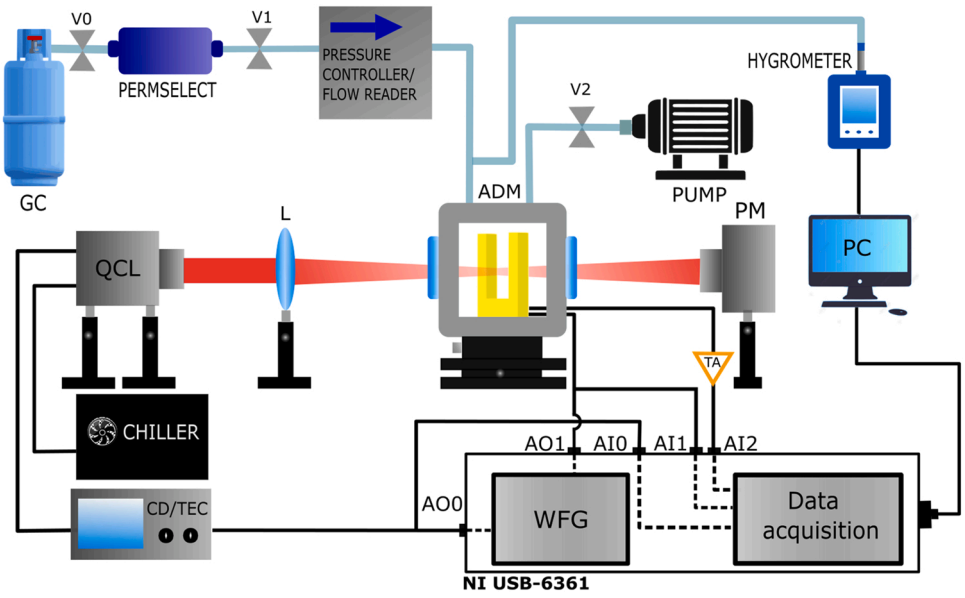

Fig. 1. Schematic of the experimental setup. QCL: quantum cascade laser, TEC: thermoelectric cooler, CD: current driver, WFG: waveform generator, AO0, AO1: analog outputs; AI0, AI1: analog: inputs; L: focusing lens, ADM: acoustic detection module, TA: transimpedance amplifier, PM: power meter, V0, V1 and V2: needle valves, DAQ: data acquisition card, PC: personal computer.

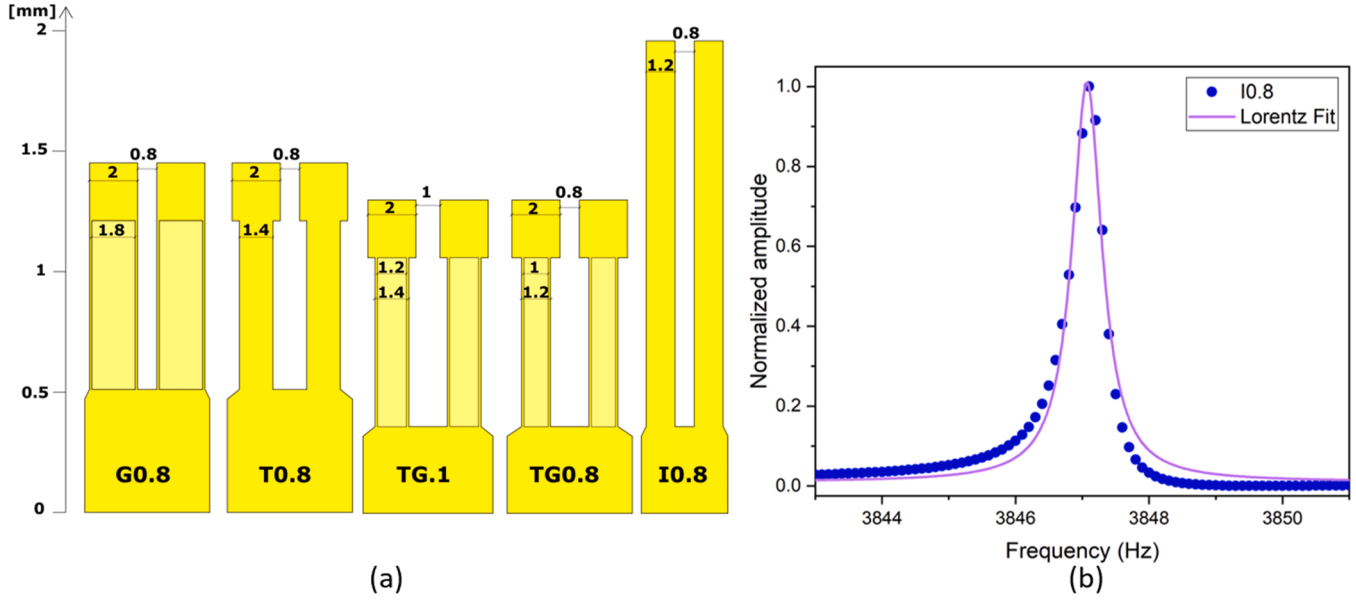

Fig. 2. (a) Schematic of the employed QTFs. All reported dimensions are in the unit of millimeters (mm). (b) Normalized resonance curve of QTF I0.8 at atmospheric pressure (blue dots) with Lorentzian fit (purple line).

recently designed with the aim of developing a low-resonance frequency QTF (between 2 kHz and 4 kHz) with a quality factor higher than the typical values (lower than 5000 at atmospheric pressure) of the currently available low-resonance frequency custom tuning forks [58]. The QTF I0.8 resonance curve obtained at atmospheric pressure is shown in Fig. 2(a), together with the Lorentzian fit.

At atmospheric pressure, the measured resonance frequency and quality factor for QTF I0.8 are 3846.57 Hz and 7050, respectively. Asymmetry in the resonance curve is ascribed to residual parasitic capacitance at the pins connection [59]. The fundamental mode resonance frequencies and quality factors at atmospheric pressure of the selected set of QTFs are summarized in Table 2.

Each selected QTF has a prong spacing greater than the DFB-QCL beam waist at the lens focal plane (∼ 400 μm) in order to reduce the

Table 2
Resonance properties of the QTFs sketched in Fig. 2(a). QTF name key: G: grooved, T: T-shaped, I: I-shaped, number: prongs spacing (in mm). f_0: fundamental mode resonance frequency at atmospheric pressure. Q: quality factor at atmospheric pressure.

QTF name	f_0 (Hz)	Q	Ref.
G0.8	15222.93	15050	[58]
T0.8	12460.55	15540	[58]
TG1	9350	9080	[60]
TG0.8	8069.96	10900	[61]
I0.8	3846.57	7050	This work

possible background noise arising from beam tails hitting the prongs of the resonators.

4. Results

4.1. Absorption lines selection

The optimum configuration to unambiguously identify and independently excite the two methane isotopologues, avoiding spectral interference, consists in a set of working parameters, including pressure and temperature of the gas sample, allowing a complete separation of the 2 f-QEPAS profiles associated with the targeted optical transitions. Moreover, the most preferable $^{12}CH_4$ absorption line should have a line-strength ~ two orders of magnitude lower than $^{13}CH_4$ to balance out their different concentrations (~ 98.9 % $^{12}CH_4$, 1.1 % $^{13}CH_4$) in a methane sample in natural abundance and to achieve a suitable detection sensitivity for both species. The cross-section dependence on temperature via ground state energies must also be comparable.

The Hitran Database was employed to simulate the absorption cross section of 1000 ppm of $^{13}CH_4$ and $^{12}CH_4$ diluted in pure N_2 within the laser emission spectral range [54]. Absorption cross section of 2400 ppm of H_2O was also simulated. The second derivative of the simulated absorption cross sections are shown in Fig. 3, at the lowest and highest working pressure, namely 50 Torr and 700 Torr, and at a room temperature of 23 °C.

The selected $^{12}CH_4$ and $^{13}CH_4$ absorption features are located at 1296.12 cm^{-1} and 1296.25 cm^{-1}, far from H_2O features, and have a line-strength of 3.97 * 10^{-24} cm/molecule and 4.57 * 10^{-23} cm/molecule, respectively. For a methane sample, having isotopologues in natural abundance, the cross-section ratio σ_{13}/σ_{12} is equal to 0.11 at 50 Torr and T = 23°, with a negligible −0.68‰/° temperature coefficient. It is worth to notice that in this spectral range QEPAS cannot be used to retrieve H_2O concentration due to the overlap with a $^{13}CH_4$ absorption feature. This justifies the use of a hygrometer to determine the temperature and relative humidity of the gas sample and to calculate the absolute humidity [33].

4.2. Measurement of vibrational-translational effective relaxation rate

As discussed in the first section, the dependence of the QEPAS signal and QTF quality factor on gas pressure can be used to recover the radiation to sound-conversion efficiency for different acoustic frequencies.

Measurements were first performed by flushing a mixture of 1000 ppm of $^{12}CH_4$, 2400 ppm of H_2O and the rest N_2 through the gas line. Each QTF was firstly electrically characterized at different working pressures, namely 50, 100, 200, 300, 400, 500, 600 and 700 Torr. The $^{12}CH_4$ QEPAS signal was acquired at the listed pressure values, optimizing the laser amplitude modulation and frequency. Measurements were repeated by flushing a mixture of 1000 ppm of $^{13}CH_4$, 2400 ppm of H_2O and the rest N_2.

As a representative, the QEPAS signal of both isotopologues measured with QTF T0.8 is shown in Fig. 4 at 50 Torr and 700 Torr.

At 700 Torr the negative lobes of the QEPAS scans of the two $^{13}CH_4$ absorption lines overlap, but the QEPAS peak of the selected line is not affected by this distortion. The $^{12}CH_4$ QEPAS signal of the 1296.19 cm^{-1} absorption line merges with the 1296.12 cm^{-1} one, leading to an asymmetry in the measured QEPAS spectrum.

The normalized QEPAS signals $^{12}CH_4$ *S* and $^{13}CH_4$ *S*, related to each isotopologue, are represented as a function of pressure in Fig. 5a and d, respectively. The uncertainty on the represented data points corresponds to the 1σ standard deviation of the signal acquired with the laser current locked on the absorption peak for about 40 s. Starting from the lowest pressure, the QEPAS signal rapidly increases until it reaches a maximum value; then it slightly decreases. This trend results from the combination of two opposite effects. The gas density increases with pressure, causing a stronger damping of the prong motion and thus a reduction of the QTF quality factor. On the other hand, the radiation-to-sound conversion efficiency increases with pressure since more collisional partners are available for energy relaxation of the excited molecules. The maxima in the graphs of Fig. 5a and d correspond to the pressure at which the tradeoff between these behaviors occurs. As an example, for $^{12}CH_4$ the highest QEPAS signal is achieved at 200 Torr for QTFs I0.8 and TG0.8 and at 300 Torr for the others. Thus, the tradeoff pressure decreases with the modulation frequency.

The ratio *S/Q* normalized to the highest value is plotted in Fig. 5b and e for the two isotopologues as a function of pressure (datapoints). Such curves represent a family of $\varepsilon(p)$ functions, each corresponding to a modulation frequency. Initially, $\varepsilon(p)$ shows an increase with pressure and then it reaches a plateau, which corresponds to a complete conversion, per oscillation cycle, of vibrational energy of the excited state into heat. The pressure at which the plateau is reached increases with *f* since more molecules are needed to have a complete energy release of the gas in one oscillation cycle. Eq. (7) was used to fit the data in Fig. 5b and d (solid lines) to retrieve the parameter A^I, which has been further plotted as a function of the modulation frequency *f* in Fig. 5c and f for the two isotopologues.

Then, the effective relaxation rate was retrieved for the two

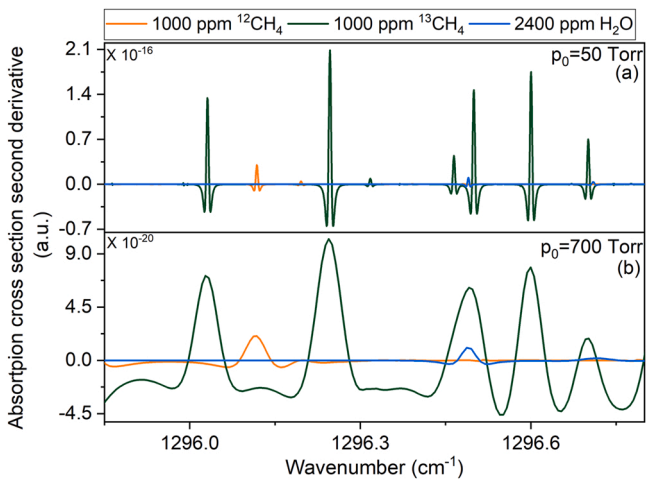

Fig. 3. Second derivative of the absorption cross section of 1000 ppm of $^{12}CH_4$ (orange), 1000 ppm of $^{13}CH_4$ (green) and 2400 ppm of H_2O (blue) in N_2, within the laser spectral range at working pressure of 50 Torr (a) and 700 Torr (b).

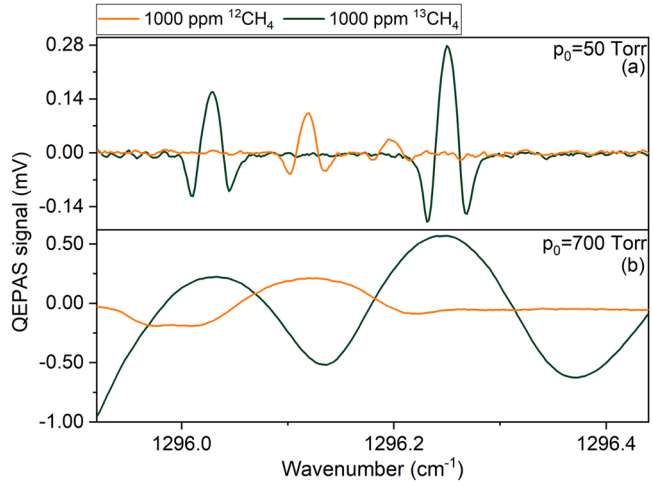

Fig. 4. QEPAS signal of 1000 ppm of $^{12}CH_4$ (orange) and $^{13}CH_4$ (green) measured in a mixture containing 2400 ppm of H_2O and the rest N_2 at 50 Torr (a) and 700 Torr (b) by employing QTF T0.8.

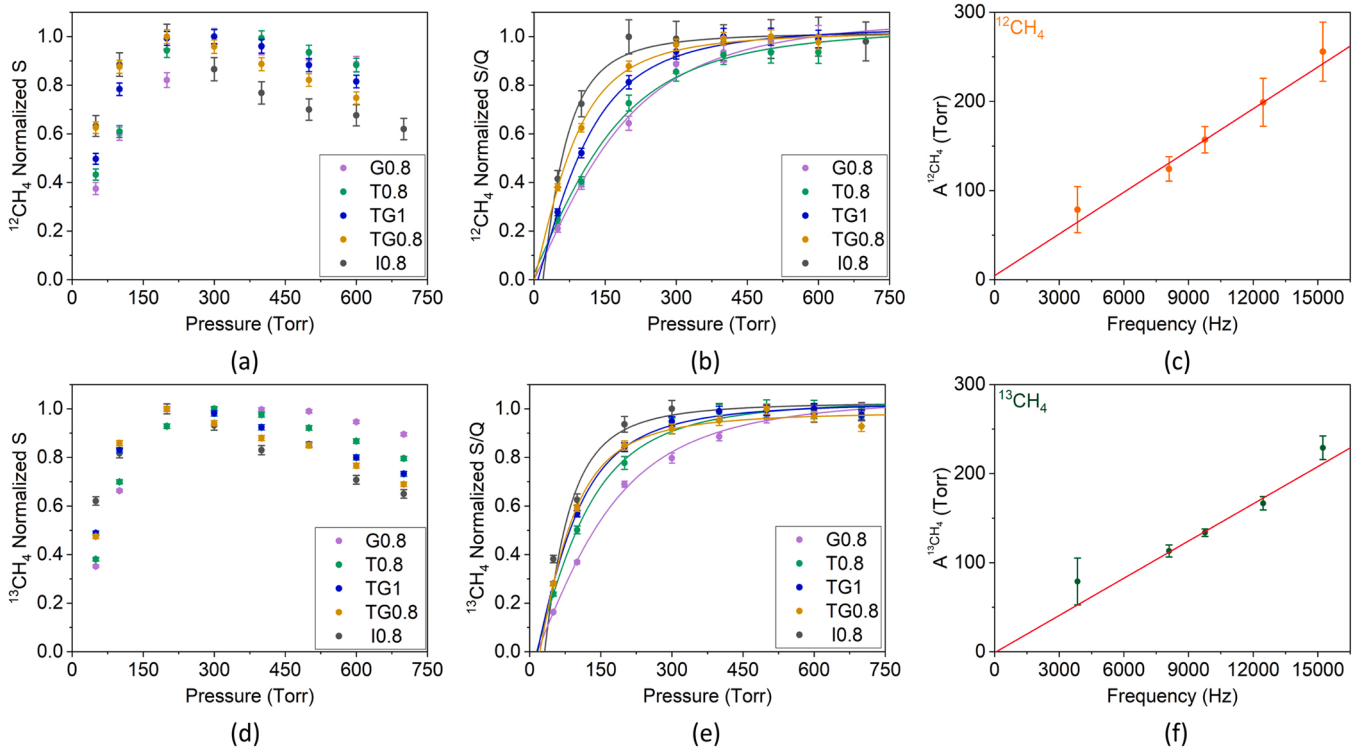

Fig. 5. Normalized QEPAS signal S as function of pressure for $^{12}CH_4$ (a) and $^{13}CH_4$ (d). Normalized S/Q data-points as a function of pressure for $^{12}CH_4$ (b) and $^{13}CH_4$ (e). The fitting curves obtained using Eq. (7) are represented as continuous lines. A^I parameter as a function of modulation frequency f for $^{12}CH_4$ (c) and $^{13}CH_4$ (f). Data are referred to a mixture containing 1000 ppm of $^{12}CH_4$ or $^{13}CH_4$, 2400 ppm of H_2O and the rest N_2.

Table 3
Comparison between the experimental effective relaxation rates of 1000 ppm of $^{12}CH_4$ and $^{13}CH_4$ in a mixture of 2400 ppm of H_2O and the rest N_2 and the theoretical effective relaxation rate of 1000 ppm of CH_4 in the same mixture, calculated employing the k values reported in Table 1.

Molecule	k (10^2 Torr^{-1}s^{-1})	Ref.
$^{12}CH_4$	4.02 ± 0.39	This work
$^{13}CH_4$	4.51 ± 0.55	This work
CH_4	4.22	Table 1

isotopologues using Eq. (6a). The obtained results are reported in Table 3, together with the theoretical values calculated employing Eq. (3) and the values of methane V-T relaxation rate reported in Table 1.

The result shows that within the fitting errors, no significant differences in measured relaxation rates were observed between the two isotopologues. Moreover, both values are in a good agreement with the effective methane relaxation rate estimated in a standard sample of CH_4 containing natural abundances of each isotopologues.

4.3. Measurement of vibrational-translational relaxation rates

A more detailed comparison between the relaxation dynamics of the two isotopologues requires measuring the relaxation rate of a $^{13}CH_4$ and $^{12}CH_4$ molecule colliding respectively with N_2 ($k_{N_2}^{^{13}CH_4}$, $k_{N_2}^{^{12}CH_4}$) and H_2O ($k_{H_2O}^{^{13}CH_4}$, $k_{H_2O}^{^{12}CH_4}$) molecules. With this aim, data in Fig. 5 were fitted considering the explicit dependence of A^I on the V-T relaxation rates, i.e., using Eqs. (5) and (6a). In this case, the fitting procedure did not converge due to the increase of number of parameters being the dataset size the same. Therefore, to enlarge the dataset a different approach was employed by acquiring the QEPAS signal related to 1000 ppm of $^{13}CH_4$ and $^{12}CH_4$, respectively, at different water vapor concentration in the mixture, with QTF G0.8. Starting from a minimum value of 1000 ppm, the water vapor content in the line was increased by varying the gas flow through valve V0 (see Fig. 1). As the humidity was gradually increased the QEPAS signal increases and reaches a plateau. This trend was observed at four different pressures, namely 100, 300, 500, and 700 Torr.

Fig. 6 shows the normalized $^{12}CH_4$ QEPAS signal as a function of the calculated absolute humidity at the four listed pressures.

The obtained curves demonstrate the dependence of the radiation to sound conversion efficiency ε on the moisture level of the gas sample. As listed in Table 1, CH_4-H_2O collisions exhibit large rates; therefore, H_2O acts as a V-T promoter for methane [62]. Consequently, the $^{12}CH_4$ PA signal increases as H_2O concentration increases until it reaches a plateau level. In this condition, the amount of water is so high that the excess of energy of optically excited CH_4* molecules is completely relaxed via CH_4-H_2O collisions. The absolute humidity at which this condition is reached decreases as the pressure increases since more molecules are available for excited molecules relaxation. For this reason, the plateau is not reached at 100 Torr, meaning that for such a low pressure, an absolute humidity greater than the one achievable with the employed experimental setup was needed to reach a saturation condition. Similar trends were obtained with $^{13}CH_4$. By fitting the experimental data with Eq. (8), parameters $B_{H_2O}^I$ and $B_{N_2}^I$ can be calculated. The obtained values for $^{12}CH_4$ are plotted as a function of pressure in Fig. 7.

A linear fit was imposed to estimate the V-T relaxation rates associated to each relaxation path in the mixture, i.e., $^{12}CH_4$* -H_2O and $^{12}CH_4$* -N_2, leading to an R^2 value of 0.993 and 0.988. The obtained values and fitting errors are summarized in Table 4, together with the results obtained from the equivalent analysis performed on 1000 ppm of $^{13}CH_4$.

The retrieved values for $^{12}CH_4$ and $^{13}CH_4$ are comparable within the errors and nearly match the theoretical values found in literature for CH_4 reported in Table 1. It is worth to notice that the effective relaxation rates calculated using Eq. (5) and the k_P^I values in Table 4 are

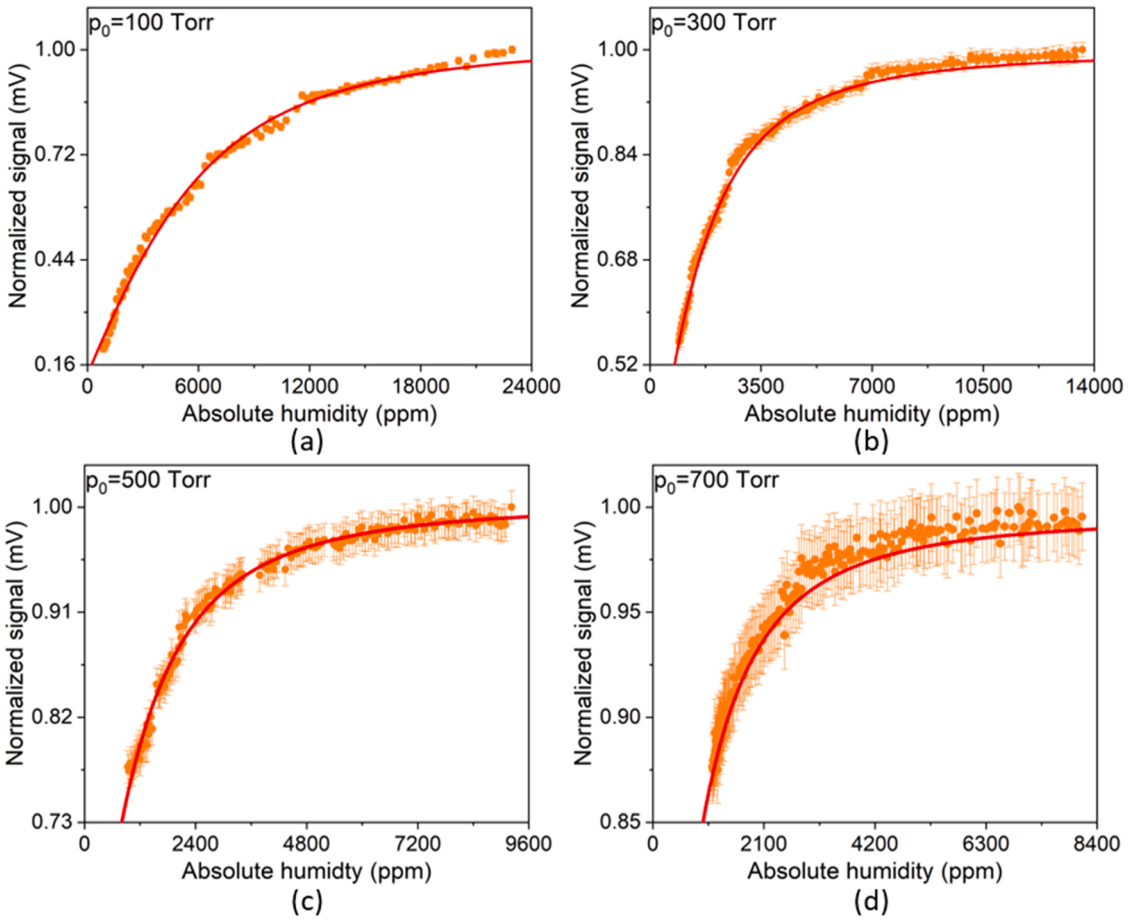

Fig. 6. Normalized $^{12}CH_4$ QEPAS signal as function of absolute humidity for the four investigated pressures.

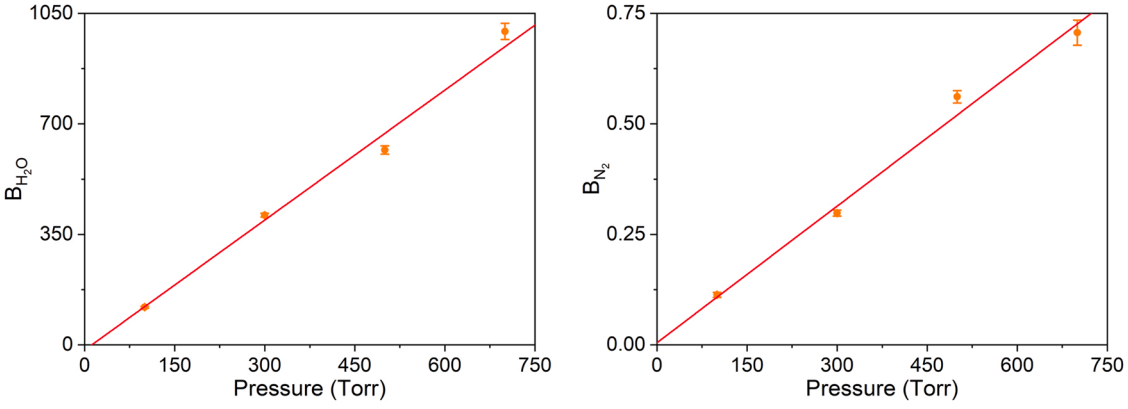

Fig. 7. Plot of the parameters $B_{H_2O}^{^{12}CH_4} = k_{H_2O}^{^{12}CH_4} p_0/2\pi f$ and $B_{N_2}^{^{12}CH_4} = k_{N_2}^{^{12}CH_4} p_0/2\pi f$ (see Eq. (8)) as a function of pressure p_0, calculated for $^{12}CH_4$. Here, $k_{H_2O}^{^{12}CH_4}$ and $k_{N_2}^{^{12}CH_4}$ are the $^{12}CH_4$ V-T relaxation rate for collisions with H_2O and N_2, respectively, and f is the modulation frequency.

Table 4
Experimental values of the V-T relaxation rates associated to collision of $^{13}CH_4$ and $^{12}CH_4$ isotopologues in the excited state with an N_2 or H_2O molecule in its ground state.

Isotopologue (I)	$k_{H_2O}^{I}$ (Torr^{-1}s^{-1})	$k_{N_2}^{I}$ (Torr^{-1}s^{-1})
$^{12}CH_4$	(1.36 ± 0.08) * 10^5	102.37 ± 7.85
$^{13}CH_4$	(1.39 ± 0.08) * 10^5	89.95 ± 9.94

$k^{^{12}CH_4} = 428 \pm 23$ Torr^{-1}s^{-1} and $k^{^{13}CH_4} = 423 \pm 24$ Torr^{-1}s^{-1}, in good agreement with the theoretical value reported for methane in natural abundance in Table 3. To evaluate how much the difference in k_P^I values between the two isotopologues could affect the measurements performed with our QEPAS setup, these values were employed to calculate the radiation-to-sound conversion efficiencies $\varepsilon^{^{12}CH_4}$ and $\varepsilon^{^{13}CH_4}$ using Eq. (2) for each selected modulation frequency, at the pressure corresponding to the highest QEPAS signal-to-noise ratio (see Fig. 5a and d). ε^I relative differences lower than 0.5 % were calculated and resulted to be in each case lower than the relative error of the signal

considering the 1-σ fluctuations for both isotopologues. Therefore, the measured difference between the k_P^I values is not expected to affect $\delta_{CH}^{13}4$ measurements performed with the employed QEPAS setup.

The obtained results can be extended for mixtures of lower methane concentrations since Eq. (5), i.e., the hypothesis of negligible self-collisions, remains valid.

5. Conclusions

In this work, the V-T relaxation rates associated to collisions of each methane isotopologue with H_2O and N_2 are measured, using mixtures containing 1000 ppm of $^{12}CH_4$ or of $^{13}CH_4$. The model is based on two assumptions: i) self-collisions are neglected, and ii) only vibrational-translational transitions from the excited state to the ground state are considered. The good agreement between the experimental trends and the theoretically predicted ones demonstrates that this assumption is valid for describing methane isotopologue relaxation in wet nitrogen-based mixtures. Firstly, the effective relaxation rates of both isotopologues were measured, by studying the dependence of the radiation-to-sound conversion efficiency on the laser modulation frequency and on the gas pressure, with a standard QEPAS setup. Then, the specific V-T relaxation time through collisions with N_2 and H_2O was determined for both isotopologues, by studying the QEPAS signal dependence on moisture level at fixed modulation frequency, at four different pressures. Both methods show that the mass difference between the two methane isotopologues and the consequent shift between their vibrational levels does not cause a significant difference between the two isotopologues relaxation rates. Consequently, when considering a mixture of methane isotopologues in a matrix of nitrogen and water, fluctuations in water or nitrogen concentration would affect in a similar way the QEPAS signal of $^{13}CH_4$ and $^{12}CH_4$ isotopologues. Thus, the isotopic ratio is not expected to change and it's not going to depend on the matrix composition.

As a future development, this study should be extended to high concentration methane samples with variable isotopic compositions. In such a case, the relaxation rates associated to self-collisions and to collisions of each isotopologue with the other one can no longer be considered negligible. The final aim is to assess and filter out the possible non-spectral cross-correlations when the fluctuations in concentration of one isotopologue can influence the measurement of the other one, leading to an accurate evaluation of the isotopic ratio of a CH_4-based sample with QEPAS technique.

Funding source

All sources of funding should also be acknowledged and you should declare any involvement of study sponsors in the study design; collection, analysis and interpretation of data; the writing of the manuscript; the decision to submit the manuscript for publication. If the study sponsors had no such involvement, this should be stated.

Declaration of Competing Interest

A conflicting interest exists when professional judgement concerning a primary interest (such as patient's welfare or the validity of research) may be influenced by a secondary interest (such as financial gain or personal rivalry). It may arise for the authors when they have financial interest that may influence their interpretation of their results or those of others. Examples of potential conflicts of interest include employment, consultancies, stock ownership, honoraria, paid expert testimony, patent applications/registrations, and grants or other funding.

Data Availability

Data will be made available on request.

Acknowledgements

The authors from Shanxi University acknowledge financial support from National Key R&D Program of China, code: 2019YFE0118200. The authors from Dipartimento Interateneo di Fisica di Bari acknowledge financial support from PNRR MUR project PE0000023-NQSTI and THORLABS GmbH within the PolySenSe joint research laboratory. Dr. Marilena Giglio acknowledges POR PUGLIA FESR-FSE 2014 / 2020 – Asse X – Azione 10.4. Research for Innovation –REFIN, code: 02BC5698. Dr. Giansergio Menduni acknowledges financial support from the Fondo Sociale Europeo REACT EU—Programma Operativo Nazionale Ricerca e Innovazione 2014–2020 by Ministero dell'Università e della Ricerca, Italy, code: D95F21002140006. Dr. Lei Dong acknowledges financial support from National Natural Science Foundation of China (NSFC), code: 62235010 , 62175137, 62122045, 62075119; The Shanxi Science Fund for Distinguished Young Scholars, code: 20210302121003.

References

[1] R.W. Howarth, A bridge to nowhere: methane emissions and the greenhouse gas footprint of natural gas, Energy Sci. Eng. 2 (2014) 47–60, https://doi.org/10.1002/ese3.35.
[2] European commission, (2022). ⟨https://energy.ec.europa.eu⟩.
[3] C. Le Fevre, Methane Emissions: from blind spot to spotlight, 2017.
[4] S. Kirschke, et al., Three decades of global methane sources and sinks, Nat. Geosci. 6 (2013) 813–823.
[5] International Energy Agency, (2022). ⟨https://www.iea.org/⟩.
[6] B.B. Bernard, J.M. Brooks, W.M. Sackett, Natural gas seepage in the Gulf of Mexico, Earth Planet. Sci. Lett. 31 (1976) 48–54.
[7] J. Aali, H. Rahimpour-Bonab, M.R. Kamali, Geochemistry and origin of the world's largest gas field from Persian Gulf, Iran, J. Pet. Sci. Eng. 50 (2006) 161–175, https://doi.org/10.1016/j.petrol.2005.12.004.
[8] T. Zhang, B.M. Krooss, Experimental investigation on the carbon isotope fractionation of methane during gas migration by diffusion through sedimentary rocks at elevated temperature and pressure, Geochim. Cosmochim. Acta 65 (2001) 2723–2742, https://doi.org/10.1016/S0016-7037(01)00601-9.
[9] O.A. Sherwood, J.D. Rogers, G. Lackey, T.L. Burke, S.G. Osborn, J.N. Ryan, Groundwater methane in relation to oil and gas development and shallow coal seams in the Denver-Julesburg Basin of Colorado, Proc. Natl. Acad. Sci. U. S. A. 113 (2016) 8391–8396, https://doi.org/10.1073/PNAS.1523267113/SUPPL_FILE/PNAS.1523267113.SAPP.PDF.
[10] S.G. Osborn, A. Vengosh, N.R. Warner, R.B. Jackson, Methane contamination of drinking water accompanying gas-well drilling and hydraulic fracturing, Proc. Natl. Acad. Sci. U. S. A. 108 (2011) 8172–8176, https://doi.org/10.1073/pnas.1100682108.
[11] J. Liu, H. Chen, Q. Zhu, Y. Shen, X. Wang, M. Wang, C. Peng, A novel pathway of direct methane production and emission by eukaryotes including plants, animals and fungi: an overview, Atmos. Environ. 115 (2015) 26–35, https://doi.org/10.1016/J.ATMOSENV.2015.05.019.
[12] M. Schroll, F. Keppler, M. Greule, C. Eckhardt, H. Zorn, K. Lenhart, The stable carbon isotope signature of methane produced by saprotrophic fungi, Biogeosciences 17 (2020) 3891–3901, https://doi.org/10.5194/BG-17-3891-2020.
[13] H. Nair, M.E. Summers, C.E. Miller, Y.L. Yung, Isotopic fractionation of methane in the martian atmosphere, Icarus 175 (2005) 32–35, https://doi.org/10.1016/J.ICARUS.2004.10.018.
[14] V.A. Krasnopolsky, J.P. Maillard, T.C. Owen, Detection of methane in the martian atmosphere: evidence for life, Icarus 172 (2004) 537–547, https://doi.org/10.1016/J.ICARUS.2004.07.004.
[15] K.R. Dominato, B.J. Rostron, M.J. Hendry, E.E. Schmeling, C.D. Sandau, S.O. C. Mundle, Developing deep high-resolution concentration and 13C isotope profiles for methane, ethane, and propane, J. Pet. Sci. Eng. 170 (2018) 280–290, https://doi.org/10.1016/J.PETROL.2018.06.064.
[16] X. Wang, C.Q. Liu, N. Zhang, S. Xu, Z. Pang, S.L. Li, H. Ding, J. Chen, Z. Xie, R. M. Ellam, Clumped methane isotopologues (13CH3D and 12CH2D2) of natural samples measured using a high-resolution mass spectrometer with an improved pretreatment system, J. Anal. . Spectrom. 38 (2022) 186–196, https://doi.org/10.1039/d2ja00315e.
[17] C. Zhang, S. Qiao, Y. Ma, Highly sensitive photoacoustic acetylene detection based on differential photoacoustic cell with retro-reflection-cavity, Photoacoustics 30 (2023), 100467, https://doi.org/10.1016/j.pacs.2023.100467.
[18] S. Qiao, A. Sampaolo, P. Patimisco, V. Spagnolo, Y. Ma, Ultra-highly sensitive HCl-LITES sensor based on a low-frequency quartz tuning fork and a fiber-coupled multi-pass cell, Photoacoustics 27 (2022), 100381, https://doi.org/10.1016/j.pacs.2022.100381.
[19] H. Lin, H. Zheng, B.A.Z. Montano, H. Wu, M. Giglio, A. Sampaolo, P. Patimisco, W. Zhu, Y. Zhong, L. Dong, R. Kan, J. Yu, V. Spagnolo, Ppb-level gas detection using on-beam quartz-enhanced photoacoustic spectroscopy based on a 28 kHz tuning fork, Photoacoustics 25 (2022), 100321, https://doi.org/10.1016/j.pacs.2021.100321.

[20] G. Leahu, R.L. Voti, S. Paoloni, C. Sibilia, M. Bertolotti, Trace gas analysis from glazes by means of a compact photothermal deflection spectroscopy apparatus, Rev. Sci. Instrum. 84 (2013), https://doi.org/10.1063/1.4848875.
[21] X. Liu, S. Cheng, H. Liu, S. Hu, D. Zhang, H. Ning, A survey on gas sensing technology, 12 (2012) 9635–9665. Sensors Vol. 12 (2012) 9635–9665, https://doi.org/10.3390/S120709635.
[22] J. Hodgkinson, R.P. Tatam, Optical gas sensing: a review, Meas. Sci. Technol. 24 (2012) 12004.
[23] C. Massie, G. Stewart, G. McGregor, J.R. Gilchrist, Design of a portable optical sensor for methane gas detection, Sens. Actuators B Chem. 113 (2006) 830–836, https://doi.org/10.1016/J.SNB.2005.03.105.
[24] P. Patimisco, A. Sampaolo, L. Dong, F.K. Tittel, V. Spagnolo, Recent advances in quartz enhanced photoacoustic sensing, Appl. Phys. Rev. 5 (2018), 011106, https://doi.org/10.1063/1.5013612.
[25] F.K. Tittel, D.V. Serebryakov, A.L. Malinovsky, I.V. Morozov, Applications of quartz tuning forks in spectroscopic gas sensing, Rev. Sci. Instrum. 27 (2002) 43105, https://doi.org/10.1364/OE.22.028222.
[26] M. Bertolotti, R.Li Voti, A note on the history of photoacoustic, thermal lensing, and photothermal deflection techniques, J. Appl. Phys. 128 (2020), https://doi.org/10.1063/5.0023836.
[27] Y. Li, R. Wang, F.K. Tittel, Y. Ma, Sensitive methane detection based on quartz-enhanced photoacoustic spectroscopy with a high-power diode laser and wavelet filtering, Opt. Lasers Eng. 132 (2020), 106155, https://doi.org/10.1016/J.OPTLASENG.2020.106155.
[28] Z. Gong, T. Gao, L. Mei, K. Chen, Y. Chen, B. Zhang, W. Peng, Q. Yu, Ppb-level detection of methane based on an optimized T-type photoacoustic cell and a NIR diode laser, Photoacoustics 21 (2021), 100216, https://doi.org/10.1016/J.PACS.2020.100216.
[29] H. Wu, L. Dong, X. Yin, A. Sampaolo, P. Patimisco, W. Ma, L. Zhang, W. Yin, L. Xiao, V. Spagnolo, S. Jia, Atmospheric CH4 measurement near a landfill using an ICL-based QEPAS sensor with V-T relaxation self-calibration, Sens. Actuators B Chem. 297 (2019), 126753, https://doi.org/10.1016/j.snb.2019.126753.
[30] A.A. Kosterev, Y.A. Bakhirkin, F.K. Tittel, S. McWhorter, B. Ashcraft, QEPAS methane sensor performance for humidified gases, Appl. Phys. B Lasers Opt. 92 (2008) 103–109, https://doi.org/10.1007/s00340-008-3056-9.
[31] S. Schilt, J.P. Besson, L. Thévenaz, Near-infrared laser photoacoustic detection of methane: the impact of molecular relaxation, Appl. Phys. B Lasers Opt. 82 (2006) 319–329, https://doi.org/10.1007/s00340-005-2076-y.
[32] V. Zéninari, B. Parvitte, D. Courtois, V.A. Kapitanov, Y.N. Ponomarev, Methane detection on the sub-ppm level with a near-infrared diode laser photoacoustic sensor, Infrared Phys. Technol. 44 (2003) 253–261, https://doi.org/10.1016/S1350-4495(03)00135-X.
[33] A. Elefante, G. Menduni, H. Rossmadl, V. Mackowiak, M. Giglio, A. Sampaolo, P. Patimisco, V.M.N. Passaro, V. Spagnolo, Environmental monitoring of methane with quartz-enhanced photoacoustic spectroscopy exploiting an electronic hygrometer to compensate the H2O influence on the sensor signal, 20 (2020) 2935, Sensors Vol. 20 (2020) 2935, https://doi.org/10.3390/S20102935.
[34] G. Menduni, A. Zifarelli, E. Kniazeva, S. Dello Russo, A.C. Ranieri, E. Ranieri, P. Patimisco, A. Sampaolo, M. Giglio, F. Manassero, E. Dinuccio, G. Provolo, H. Wu, D. Lei, V. Spagnolo, Measurement of methane, nitrous oxide and ammonia in atmosphere with a compact quartz-enhanced photoacoustic sensor, Sens. Actuators B. Chem. 375 (2023), 132953, https://doi.org/10.1016/j.snb.2022.132953.
[35] A. Zifarelli, G. Menduni, M. Giglio, A. Elefante, A. Sukhinets, A. Sampaolo, P. Patimisco, S. Fangyuan, W. Chongwu, Q.J. Wang, V. Spagnolo, Compact and versatile QEPAS-based sensor box for simultaneous detection of methane and infrared absorber gas molecules in ambient air, Front. Environ. Chem. 3 (2022) 1–11, https://doi.org/10.3389/fenvc.2022.926233.
[36] L. Dong, J. Wright, B. Peters, B.A. Ferguson, F.K. Tittel, S. McWhorter, Compact QEPAS sensor for trace methane and ammonia detection in impure hydrogen, Appl. Phys. B Lasers Opt. 107 (2012) 459–467, https://doi.org/10.1007/S00340-012-4908-X/FIGURES/12.
[37] M. Jahjah, W. Ren, P. Stefá, R. Lewicki, J. Zhang, W. Jiang, J. Tarka, F.K. Tittel, A compact QCL based methane and nitrous oxide sensor for environmental and medical applications (2014), https://doi.org/10.1039/c3an01452e.
[38] A. Sampaolo, G. Menduni, P. Patimisco, M. Giglio, V.M.N. Passaro, L. Dong, H. Wu, F.K. Tittel, V. Spagnolo, Quartz-enhanced photoacoustic spectroscopy for hydrocarbon trace gas detection and petroleum exploration, Fuel 277 (2020), 118118, https://doi.org/10.1016/j.fuel.2020.118118.
[39] P. Luo, J. Harrist, G. Menduni, R. Mesdour, N. Stmichel, A. Sampaolo, Simultaneous detection of methane, ethane, and propane by QEPAS sensors for on-site hydrocarbon characterization and production monitoring, ACS Omega 7 (2022) 3395–3406, https://doi.org/10.1021/acsomega.1c05645.
[40] A. Sampaolo, P. Patimisco, M. Giglio, A. Zifarelli, H. Wu, L. Dong, V. Spagnolo, Quartz-enhanced photoacoustic spectroscopy for multi-gas detection: a review, Anal. Chim. Acta (2021), 338894.
[41] G. Menduni, F. Sgobba, S. Dello Russo, A.C. Ranieri, A. Sampaolo, P. Patimisco, M. Giglio, V.M.N. Passaro, S. Csutak, D. Assante, E. Ranieri, E. Geoffrion, V. Spagnolo, Fiber-coupled quartz-enhanced photoacoustic spectroscopy system for methane and ethane monitoring in the near-infrared spectral range, Molecules 25 (2020) 1–12, https://doi.org/10.3390/molecules25235607.
[42] M.-S. Bahr, M. Wolff, PAS-based isotopologic analysis of highly concentrated methane, Front. Environ. Chem. 26 (2022), https://doi.org/10.3389/FENVC.2022.1029708.
[43] A. Loh, M. Wolff, Multivariate analysis of photoacoustic spectra for the detection of short-chained hydrocarbon isotopologues, Molecules 25 (2020), https://doi.org/10.3390/molecules25092266.
[44] A. Loh, M. Wolff, High resolution spectra of 13C ethane and propane isotopologues photoacoustically measured using interband cascade lasers near 3.33 and 3.38 μm, respectively, J. Quant. Spectrosc. Radiat. Transf. 227 (2019) 111–116, https://doi.org/10.1016/j.jqsrt.2019.01.027.
[45] G. Wysocki, A.A. Kosterev, F.K. Tittel, Influence of molecular relaxation dynamics on quartz-enhanced photoacoustic detection of CO_2 at λ =2 μm, 2006 852, Appl. Phys. B 85 (2006) 301–306, https://doi.org/10.1007/S00340-006-2369-9.
[46] P. Repond, M.W. Sigrist, Photoacoustic spectroscopy on trace gases with continuously tunable CO_2 laser, Appl. Opt. 35 (1996) 4065, https://doi.org/10.1364/AO.35.004065.
[47] M. Olivieri, G. Menduni, M. Giglio, A. Sampaolo, P. Patimisco, H. Wu, L. Dong, V. Spagnolo, Characterization of H 2 S QEPAS detection in methane-based gas leaks dispersed into environment, Photoacoustics 29 (2023), 100438, https://doi.org/10.1016/j.pacs.2022.100438.
[48] M. Müller, T. Rück, S. Jobst, J. Pangerl, S. Weigl, R. Bierl, F.M. Matysik, An algorithmic approach to compute the effect of non-radiative relaxation processes in photoacoustic spectroscopy, Photoacoustics 26 (2022), 100371, https://doi.org/10.1016/j.pacs.2022.100371.
[49] G. Menduni, A. Zifarelli, A. Sampaolo, P. Patimisco, M. Giglio, N. Amoroso, H. Wu, L. Dong, R. Bellotti, V. Spagnolo, High-concentration methane and ethane QEPAS detection employing partial least squares regression to filter out energy relaxation dependence on gas matrix composition, Photoacoustics 26 (2022), 100349, https://doi.org/10.1016/j.pacs.2022.100349.
[50] S. Dello Russo, A. Sampaolo, P. Patimisco, G. Menduni, M. Giglio, C. Hoelzl, V.M.N. Passaro, H. Wu, L. Dong, V. Spagnolo, Quartz-enhanced photoacoustic spectroscopy exploiting low-frequency tuning forks as a tool to measure the vibrational relaxation rate in gas species, Photoacoustics 21 (2021), 100227, https://doi.org/10.1016/j.pacs.2020.100227.
[51] O.N. Ulenikov, E.S. Bekhtereva, S. Albert, S. Bauerecker, H.M. Niederer, M. Quack, Survey of the high resolution infrared spectrum of methane (12CH4 and 13CH4): Partial vibrational assignment extended towards 12 000 cm-1 (2014), https://doi.org/10.1063/1.4899263.
[52] A. Miklos, P. Hess, Modulated and pulsed photoacoustics in trace gas analysis, Anal. Chem. 72 (2000) 30–37.
[53] M. Olivieri, A. Zifarelli, G. Menduni, M. Di Gioia, C. Marzocca, V.M.N. Passaro, A. Sampaolo, M. Giglio, V. Spagnolo, P. Patimisco, Influence of air pressure on the resonance properties of a t-shaped quartz tuning fork coupled with resonator tubes, Appl. Sci. 11 (2021), https://doi.org/10.3390/app11177974.
[54] I.E. Gordon, L.S. Rothman, C. Hill, R.V. Kochanov, Y. Tan, P.F. Bernath, M. Birk, V. Boudon, A. Campargue, K.V. Chance, B.J. Drouin, J.M. Flaud, R.R. Gamache, J. T. Hodges, D. Jacquemart, V.I. Perevalov, A. Perrin, K.P. Shine, M.A.H. Smith, J. Tennyson, G.C. Toon, H. Tran, V.G. Tyuterev, A. Barbe, A.G. Császár, V.M. Devi, T. Furtenbacher, J.J. Harrison, J.M. Hartmann, A. Jolly, T.J. Johnson, T. Karman, I. Kleiner, A.A. Kyuberis, J. Loos, O.M. Lyulin, S.T. Massie, S.N. Mikhailenko, N. Moazzen-Ahmadi, H.S.P. Müller, O.V. Naumenko, A.V. Nikitin, O.L. Polyansky, M. Rey, M. Rotger, S.W. Sharpe, K. Sung, E. Starikova, S.A. Tashkun, J. Vander Auwera, G. Wagner, J. Wilzewski, P. Wcisło, S. Yu, E.J. Zak, The HITRAN2016 molecular spectroscopic database, J. Quant. Spectrosc. Radiat. Transf. 203 (2017) 3–69, https://doi.org/10.1016/J.JQSRT.2017.06.038.
[55] A.A. Kosterev, T.S. Mosely, F.K. Tittel, Impact of humidity on quartz-enhanced photoacoustic spectroscopy based detection of HCN, Appl. Phys. B Lasers Opt. 85 (2006) 295–300, https://doi.org/10.1007/s00340-006-2355-2.
[56] C. Boursier, J. Ménard, L. Doyennette, F. Menard-Bourcin, Rovibrational relaxation of methane in CH4- N2 mixtures: time-resolved IR- IR double-resonance measurements at 193 K and kinetic modeling, J. Phys. Chem. A 107 (2003) 5280–5290.
[57] P. Patimisco, A. Sampaolo, Y. Bidaux, B. Alfredo, M. Scott, J. Jiang, A. Muller, J. Faist, F.K. Tittel, V. Spagnolo, Purely wavelength- and amplitude-modulated quartz-enhanced photoacoustic spectroscopy, Opt. Express 24 (2016) 2079–2087.
[58] P. Patimisco, A. Sampaolo, M. Giglio, S. dello Russo, V. Mackowiak, H. Rossmadl, A. Cable, F.K. Tittel, V. Spagnolo, Tuning forks with optimized geometries for quartz-enhanced photoacoustic spectroscopy, Opt. Express 27 (2019) 1401–1415, https://doi.org/10.1364/OE.27.001401.
[59] M. Lee, B. Kim, S. An, W. Jhe, Dynamic responses of electrically driven quartz tuning fork and qPlus sensor: a comprehensive electromechanical model for quartz tuning fork, Sens. (Switz.) 19 (2019), https://doi.org/10.3390/s19122686.
[60] Y. Ma, Y. He, P. Patimisco, A. Sampaolo, S. Qiao, X. Yu, F.K. Tittel, V. Spagnolo, Ultra-high sensitive trace gas detection based on light-induced thermoelastic spectroscopy and a custom quartz tuning fork, Appl. Phys. Lett. 116 (2020), https://doi.org/10.1063/1.5129014.
[61] B. Sun, A. Zifarelli, H. Wu, S. Dello Russo, S. Li, P. Patimisco, L. Dong, V. Spagnolo, Mid-infrared quartz-enhanced photoacoustic sensor for ppb-Level CO detection in a SF6Gas matrix exploiting a T-grooved quartz tuning fork, Anal. Chem. 92 (2020) 13922–13929, https://doi.org/10.1021/acs.analchem.0c02772.
[62] J. Finzi, F.E. Hovis, V.N. Panfilov, P. Hess, C. Bradley Moore, Vibrational relaxation of water vapor, J. Chem. Phys. 67 (1977) 4053–4061, https://doi.org/10.1063/1.435379.

Mariagrazia Olivieri obtained the M.S. degree (cum laude) in Physics in 2021 from the University of Bari. Since October 2021, she is a PhD student at the Physics Department of the University of Bari carrying out her research work at PolySense Lab, joint-research laboratory between Technical University of Bari and THORLABS GmbH. Currently, her research activities are focused on the development of gas sensors based on Quartz Enhanced Photoacoustic spectroscopy for the analysis of complex gas mixtures.

Marilena Giglio received the M.S. degree (cum laude) in Applied Physics in 2014, and the PhD Degree in Physics in 2018 from the University of Bari. Since 2021, she is a Assistant Professor at the Physics Department of the Technical University of Bari. Her research activity is focused on the development of gas sensors based on Quartz-Enhanced Photoacoustic Spectroscopy and on the optical coupling of hollow-core waveguides with interband- and quantum-cascade lasers.

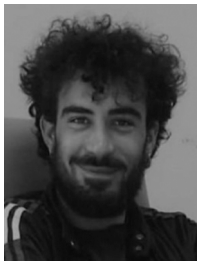

Stefano Dello Russo obtained his M.S. degree (cum laude) in Physics in 2018 from the University of Bari. From the same year, he is a PhD student at the Physics Department of the University of Bari, developing his research work at PolySense Lab, joint-research laboratory between Technical University of Bari and THORLABS GmbH. Currently, he is working as researcher at the Italian Space Agency.

Giansergio Menduni received the M.S. degree (cum laude) in Electronic Engineering in 2017 from the Technical University of Bari. Since 2018, he is a PhD student at the Electric and Information Engineering Department of Polytechnic of Bari. Since 2022, he is an Assistant Professor in Applied Physics at the Physics Department of Polytechnic of Bari. His research activity is focused on the development of gas sensors based on Quartz Enhanced Photoacoustic Spectroscopy.

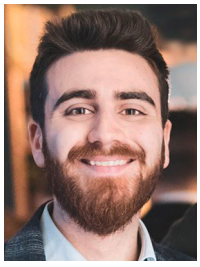

Andrea Zifarelli received the M.S. degree (cum laude) in Physics in 2018 from the University of Bari and his Ph.D. in Physics from the University of Bari in 2022. His research activities were mainly focused on the development of spectroscopic techniques based on laser absorption for the analysis of complex gas mixtures by employing quartz tuning forks as sensitive elements. This investigation was performed by using innovative laser sources as well as developing new algorithms for multivariate analysis approaches. Currently, his research activities are carried out at the PolySenSe Lab, joint-research laboratory between Technical University of Bari and THORLABS GmbH.

Pietro Patimisco obtained the Master degree in Physics (cum laude) in 2009 and the PhD Degree in Physics in 2013 from the University of Bari. Since 2023, he is an associate professor at the Physics Department of University of Bari. He was a visiting scientist in the Laser Science Group at Rice University in 2013 and 2014. The main scientific skills of Pietro Patimisco are related to the development of spectroscopic techniques for studying the light-matter interaction in the infrared range. Prof. Pietro Patimisco is co-founder of "PolySenSe Innovations", a company devoted to the development of optical-based sensors.

Angelo Sampaolo obtained his Master degree in Physics in 2013 and the PhD Degree in Physics in 2017 from University of Bari. He was an associate researcher in the Laser Science Group at Rice University from 2014 to 2016 and associate researcher at Shanxi University since 2018. Since 2019, he is Assistant Professor at Polytechnic of Bari. His research activity has focused on the development of innovative techniques in trace gas sensing, based on Quartz-Enhanced Photoacoustic Spectroscopy and covering the full spectral range from near-IR to THz.

Hongpeng Wu received his Ph.D. degree in atomic and molecular physics from Shanxi University, China, in 2017. From September, 2015 to October, 2016, he studied as a joint Ph.D. student in the Electrical and Computer Engineering Department and Rice Quantum Institute, Rice University, Houston, USA. Currently he is a professor in the Institute of Laser Spectroscopy of Shanxi University. His research interests include gas sensors, photoacoustic spectroscopy, photothermal spectroscope and laser spectroscopy techniques

Lei Dong received his Ph.D. degree in optics from Shanxi University, China, in 2007. From June, 2008 to December, 2011, he worked as a post-doctoral fellow in the Electrical and Computer Engineering Department and Rice Quantum Institute, Rice University, Houston, USA. Currently he is a professor in the Institute of Laser Spectroscopy of Shanxi University. His research interests include optical sensors, trace gas detection, photoacoustic spectroscopy and laser spectroscopy.

Vincenzo Spagnolo received the degree (summa cum laude) and the PhD, both in physics, from University of Bari. He works as Full Professor of Applied Physics at the Technical University of Bari. In 2019, he become Vice-Rector of the Technical University of Bari, deputy to Technology Transfer. Since 2017, he is the director of the joint-research lab PolySense, created by THORLABS GmbH and Technical University of Bari, devoted to the development and implementation of novel gas sensing techniques and the realization of highly sensitive QEPAS trace-gas sensors.